

NON-THERMAL BREMSSTRAHLUNG AS THE DOMINANT HARD X-RAY CONTINUUM MECHANISM FOR THE SUPERNOVA REMNANT MSH14-6 β (RCW 86)

Jacco Vink^{1,2}, Johan A. M. Bleeker, Jelle S. Kaastra, Kurt van der Heyden³, Andrew Rasmussen¹, John Dickel⁴

¹Columbia Astrophysics Laboratory, Columbia University, MC 5247, 550 W 120th street, New York, NY 10027, USA

²Chandra fellow

³SRON National Institute for Space Research, Sorbonnelaan 2, NL-3584 CA, Utrecht, The Netherlands

⁴Astronomy Department, University of Illinois, 1002 West Green Street, Urbana, IL 61801, USA

ABSTRACT

We present an analysis of the X-ray emission of the supernova remnant MSH14-6 β , which was partially covered by four observations with XMM-Newton. The detection of Fe K emission at 6.4 keV, and the lack of spatial correlation between hard X-ray and radio emission is evidence against a dominant X-ray synchrotron component. We argue that the hard X-ray continuum is best explained by non-thermal bremsstrahlung from a supra-thermal tail to an otherwise cool electron gas. The existence of low electron temperatures, required to explain the absence of line emission, is supported by low temperatures found in other parts of the remnant, which are as low as 0.2 keV in some regions.

Key words: ISM: individual (G315.4-2.3) – supernova remnants – X-rays: ISM

1. INTRODUCTION

The lack of bright emission lines in the X-ray spectra of some shell-type supernova remnants has, for the last few years, been attributed to the presence of X-ray synchrotron radiation. The best known example, and the first shell-type remnant for which X-ray synchrotron radiation was claimed, is the remnant of SN 1006 (Koyama et al. 1995).

Indeed, the small equivalent widths of X-ray emission lines from the remnant MSH14-6 β (also named RCW 86 or G315.4-2.3) based upon ASCA observations (Vink et al. 1997), was reinterpreted by Borkowski et al. (2001) as due to the presence of a synchrotron component. Additional support for this idea was provided by an apparent spatial correlation between the hard, continuum dominated X-ray emission and the radio synchrotron emission.

However, the presence of Fe K line emission at 6.4 keV complicates the interpretation of the hard X-ray continuum. This emission is the result of inner-shell ionizations of neutral or mildly ionized iron, followed by K shell fluorescence. Under-ionization can also account for the lack of emission lines from the helium and hydrogen like ionization stages of Ne, Mg, Si, S, which dominate the line

spectra of young remnants like Tycho and Cas A. These elements have a lower fluorescence yield than Fe.

Under-ionization can occur if the plasma is far out of ionization equilibrium, or it may be the result of a low electron temperature, possibly caused by insufficient electron-ion temperature equilibration (Itoh 1984). In the latter case the presence of additional energetic electrons is required for the Fe K emission, which should also give rise to non-thermal bremsstrahlung. Such non-Maxwellian particle distributions are thought to be the result of collisionless shock heating (Bykov & Uvarov 1999)

Here we present additional evidence for non-thermal bremsstrahlung based on XMM-Newton observations of MSH14-6 β . We refer to Dyer et al. (2002) for a different, Chandra, vision on the hard X-ray emission from this remnant.

2. OBSERVATION AND DATA REDUCTION

XMM-Newton (Jansen et al. 2001) observed the Southeast and Northwest of MSH14-6 β on August 17 and 18, 2000, and the Southwest on August 18, 2001. The effective exposure times are approximately 12 ks for the Southwest, 17 ks for the Southeast, and 12 ks for the two pointing towards the Northwest of the remnant. We discuss here primarily the X-ray emission from the Southeast and Northwest of the remnant. The analysis of the Southwestern part of the remnant is still in a preliminary phase.

Most of the results presented here are based on data from the European Photon Imaging Camera (EPIC), consisting of three CCD cameras MOS1 and MOS2, and the PN. The latter has the largest effective area, as it is behind the mirror that is not partially blocked by the reflective grating spectrometer (RGS), and the detector has a higher quantum efficiency (Strüder et al. 2001). Observations were made with the medium-thick filter in place, which serves to block ultra-violet contamination.

Satellite data were converted to cleaned event lists using SAS, the standard XMM-Newton software package. Images and spectra were extracted from the event lists, using only the standard event patterns 0 for PN, and 0-12 for MOS. This allowed the use of standard spectral response matrices.

For the background correction of the spectra we used the publicly available, standard, background event files.

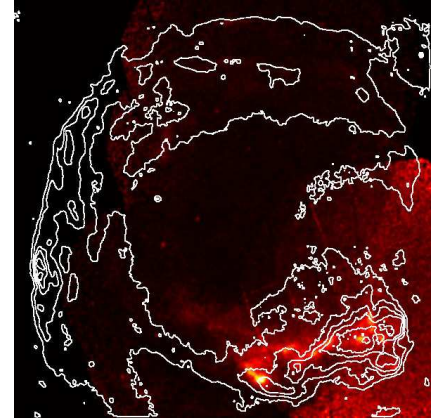
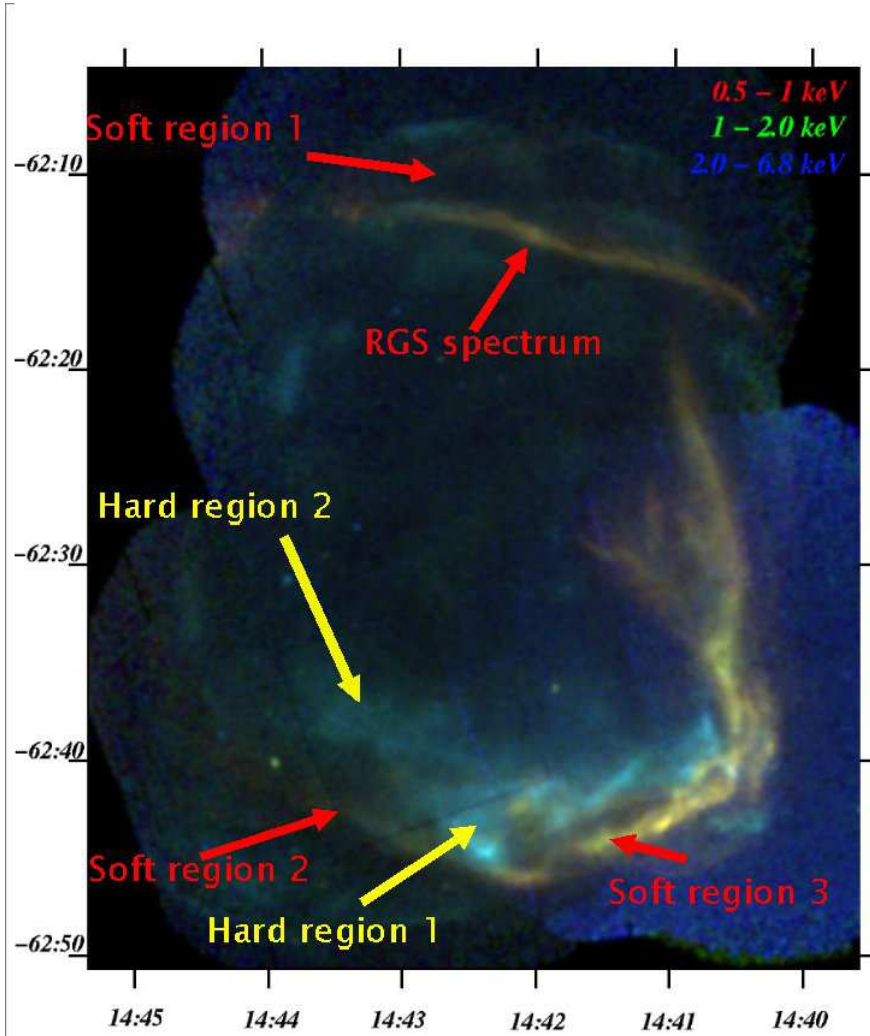


Figure 1. Mosaic of exposure corrected EPIC PN and MOS images covering the SW, SE and NW of MSH14-63. The color coding is as follows. Red : 0.54-1.0 keV; green: 1.0 -1.95 keV; blue: 1.95-6.8 keV. The labels are referred to in the text and in Fig. 2. The figure on the right shows the 1.95-6.8 keV X-ray emission with radio emission as observed by ATCA (Dickel et al. 2000) overlaid in contours.

Unfortunately, these consist of observations taken with the thin filter, possibly resulting in a background overestimation at low photon energies. We therefore used additional off-center fields of the publicly available observation of G21.5-0.9, a small supernova remnant, which was observed with the medium filter. In practice we only used these data to estimate the background for the soft X-ray emission from the Southeast of MSH14-63.

3. DATA ANALYSIS

Fig. 1 shows a mosaic of the EPIC observations. It illustrates the dramatic change in morphology going from energies of 0.5-1 keV to those > 1 keV, in more detail than previously observed by ASCA and BeppoSAX (Vink et al. 1997; Bocchino et al. 2000). As shown in Fig. 2a, the spectra of the soft X-ray regions are dominated by emission lines of O VII, O VIII, Fe XVII and Ne IX, with some spatial variation in relative strength of the line emission. This is illustrated with better resolution by the RGS spectrum of the narrow, bright shell in the Northwest of MSH14-63 (Fig. 2c).

The presence of O VII is especially indicative of a low ionization, which is the result of a low electron temperature, and/or a small ionization time¹. A lower limit to the electron temperature is obtained by assuming collisional ionization equilibrium (CIE). This gives temperatures for the spectra in Fig. 2 between 0.10 keV and 0.17 keV, see Table 1.² More realistic non-equilibrium ionization (NEI) models result in higher temperature estimates and somewhat better spectral fits (Table 1). Although there are still discrepancies between the NEI models and the data, possibly as a result of sharp density and temperature gradients and projection effects, they indicate that at least some regions have electron temperatures as low as 0.2 keV.

These temperatures are lower than indicated by the ASCA and the BeppoSAX data, but in accordance with

¹ This is usually quantified by $n_e t$, where n_e is the electron density, and t is the time since the plasma has been shocked.

² The spectral range was confined to 0b.5-1 keV, which is dominated by line emission. We used the *mekal* CIE model (Mewe et al. 1995), and the *SPEX* NEI model, which is based on the *mekal* model.

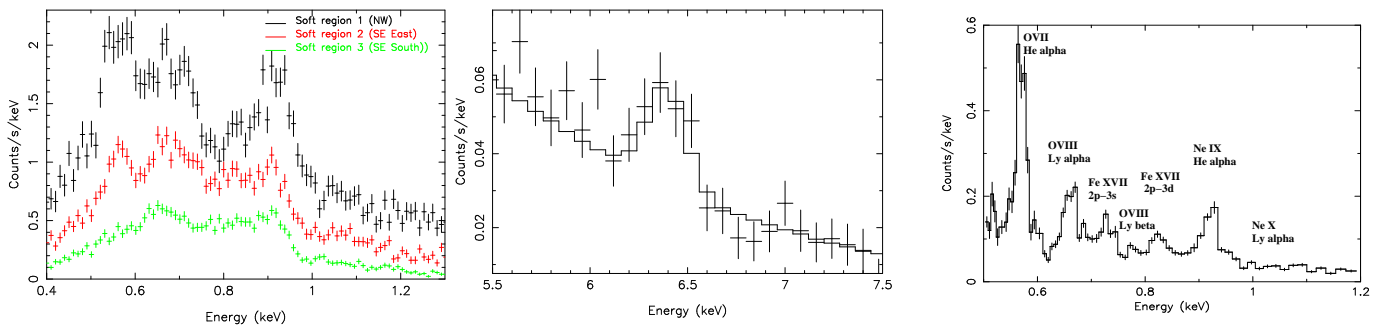


Figure 2. a) Three EPIC PN spectra arbitrary normalized to show a sequence of increasing ionization from top to bottom. The labels refer to the regions indicated in Fig. 1. b) Part of the EPIC-PN spectra from the total hard X-ray emitting region in the Southeast, showing Fe K emission around 6.4 keV, indicating underionized iron. c) The first order RGS spectrum of the Northwestern rim, with labels identifying the line emission (cf. Fig. 2a).

the ROSAT PSPC data of the Northwestern rim (Bocchino et al. 2000). The electron temperatures are also consistent with shock velocities of 310 - 605 km/s, inferred from the width of the H α and H β lines, which, under the assumption of full electron-ion equilibration (Ghavamian 1999; Ghavamian et al. 2001), translates into shock velocities of 310 - 605 km/s, and post shock gas temperatures of 0.11 - 0.42 keV.

Spectra from regions dominated by hard X-ray emission are characterized by a dominant continuum and very faint line emission. The spectrum from “hard region 1”, which is one of the brightest hard X-ray emitting regions, shows more prominent line emission than from “hard region 2”. It is not clear whether the more prominent line emission is something intrinsic to this bright X-ray knot, or that this is caused by a superposition of a soft X-ray emitting region, as this part of MSH14-63 has a complicated morphology. Good heuristic fits to the hard X-ray spectra consist of a power law continuum and a thermal components, but currently the spectral quality of this very diffuse component is not good enough to determine for instance whether the emission lines come from a plasma out of ionization-equilibrium. Clearly, the appearance of the hard spectra in itself can be explained by X-ray synchrotron emission, with the line emission belonging to the thermal plasma, which is superimposed on the hard synchrotron continuum, but the XMM-Newton data show that there are two problems with this interpretation.

The first problem is that the hard X-ray emitting region in the Southeast as a whole shows evidence for Fe K shell emission at 6.4 keV (Fig. 2). This confirms the ASCA detection of Fe K emission, but for a different region, and with a lower equivalent width of 0.24 keV. Model calculations show that for a solar iron abundance the measured equivalent width is consistent with electron temperatures in excess of ~ 3 keV, and/or a power law electron distribution with an electron index $\lesssim 3$.³ Therefore, only if

³ The calculations involved the numerical integration of an electron distribution with the (almost) neutral iron cross sec-

the iron abundance is more than the solar value, can the continuum be dominated by X-ray synchrotron emission.

The second problem is the lack of detailed spatial correlation between hard X-ray and radio emission, see for example (Fig. 1 right) the faint but distinct hard X-ray emission, labeled “hard region 2”, which lies inside the radio shell. This is in contradiction with the spatial correlation reported by Borkowski et al. (2001), based on lower spatial resolution data. In fact, the region with the hardest X-ray emission (hard region 2) has such weak radio emission, that it is difficult to determine the radio flux density from the ATCA and MOST images (Dickel et al. 2000), as these synthesis radio telescopes have sidelobes from brighter parts of the remnant which result in a negative flux density at this location. However, we have derived an upper limit of < 0.5 Jy at 1 GHz based on these images and on a 5-GHz radio image made with the single-dish Parkes telescope (Milne & Dickel 1975), using the generally accepted radio spectral index of -0.6 and total flux density of 49 Jy at 1 GHz (Green 2000).

Fitting the X-ray spectrum of this region with a power law spectrum and a thermal (CIE) spectrum yields a flux density at 1 keV ($2.4 \cdot 10^{17}$ Hz) of $1.6 \cdot 10^{-6}$ Jy. Connection of the radio and X-ray flux density gives a spectral index of ≥ -0.65 , which is remarkably close to the radio spectral index of -0.6, giving the fact that the two frequencies encompass eight orders of magnitude. This does not rule out X-ray synchrotron emission, but it is peculiar that for this particular region synchrotron losses are almost absent, whereas the radio regions are dominated by thermal soft X-ray emission; see for example the northern shell, and the ridge of radio emission connecting the southeastern and the northeastern shell, the region labeled “soft region 2” in Fig. 1. Note that the hard X-ray regions lie inside the main shell, which is a different spatial arrangement

tions, and the bremsstrahlung gaunt factors proposed by Haug (1997). The Lotz formula was used for Fe K shell ionization cross sections, and an approximate fluorescence yield of 0.3 was assumed (see e.g. Mewe (1999)).

than for SN 1006, where the X-ray synchrotron emission seems confined to a region close to the shock front, and is highly limb brightened (Koyama et al. 1995).

4. SUMMARY AND CONCLUSIONS

We have presented spatially resolved XMM-Newton spectroscopy of the supernova remnant MSH14-6 β , which shows that the hard X-ray emission is not correlated with the radio emission. Fe K emission at 6.4 keV is also present. Both observations contradict the idea that the hard X-ray emission is dominated by synchrotron radiation.

The Fe K emission indicates the presence of electrons with energies in excess of the ionization threshold ($\gtrsim 7$ keV), but these electrons should also give rise to bremsstrahlung. A *non-thermal* electron distribution seems likely, as a *thermal* distribution requires electron temperatures $kT_e > 3$ keV, which is at odds with both the measured shock velocities (Ghavamian 1999) and the electron temperatures of the regions dominated by soft X-ray emission.

Not discussed so far is the lack of line emission from O VII, which requires that the energetic electrons are part of an otherwise very cool electron distribution ($kT_e < 30$ eV). Although we presented evidence for very low temperatures this clearly deserves future attention. Moreover, as most electrons have low energies it means that the electron density is probably much higher than indicated by the X-ray data. Low temperatures may be the result of insufficient electron-ion temperature equilibration. Evidence for weak electron-ion equilibration was obtained from UV spectroscopy of SN 1006, indicating $T_e \sim 0.05T_i$, where T_i is the ion temperature (Laming et al. 1996). Recent calculations of ionization fractions for non-thermal electron distributions show that the ion fractions are quite similar to those of the equivalent temperature of the Maxwellian part of the distribution, provided that the plasma is not in ionization equilibrium, as is usually the case in supernova remnants (Porquet et al. 2001). Clearly, more model calculations are needed to assess the effects of non-thermal electron distributions on the line emission.

The evidence for non-thermal bremsstrahlung, raises the question whether other remnants may not have a similar X-ray component. This may be true, but in general it is hard to judge from hard X-ray tails alone whether the emission is non-thermal bremsstrahlung or X-ray synchrotron emission. The situation in MSH14-6 β is more fortunate, as the overall electron temperature is relatively cool, which causes the energetic electrons to betray themselves by causing Fe K fluorescence emission. Moreover, it is possible that we observe MSH14-6 β during a special period in its evolution, as non-thermal electron distributions can only exist for a time scale comparable to the electron self-equilibration time scale ($\tau_{ee} \sim 10^8/n_e$ s, see Itoh 1984). This suggests that the extreme properties of the X-ray emission from this remnant may be related to a recent interaction of the blast wave with the steep density

Table 1. Summary of spectral fits to the spectra of Fig. 2a. The degrees of freedom were 47 for CIE models (i.e. no entry in column 3) and 46 for NEI models. Elemental abundances were assumed to be solar. Labels refer to Fig. 1.

	kT_e keV	$\log(n_e t)$ cgs	norm 10^{13} cm^{-5}	N_H 10^{21} cm^{-2}	χ^2
Soft 1	$0.088^{+0.03}_{-0.01}$	-	114^{+136}_{-104}	9.0 ± 0.1	140
	0.14 ± 0.01	11.6 ± 0.2	$3.3^{+1.3}_{-1.1}$	6.9 ± 0.2	106
Soft 2	0.15 ± 0.01	-	1.2 ± 0.3	6.7 ± 0.2	159
	0.37 ± 0.10	10.3 ± 0.2	$0.06^{+0.08}_{-0.03}$	5.1 ± 0.5	60
Soft 3	0.17 ± 0.1	-	1.6 ± 0.6	6.9 ± 0.1	105
	1.1 ± 0.6	9.9 ± 0.1	$0.02^{+0.02}_{-0.01}$	4.2 ± 0.5	93

gradients associated with the wall of a wind blown cavity, as suggested by Vink et al. (1997).

Clearly, the nature of the X-ray emission and its relation to the environment of MSH14-6 β is far from solved, as a comparison of this study with Dyer et al. (2002) shows. However, more detailed imaging of the Fe K emission and possible similar inner shell ionization lines from Si K, may provide clear enough signatures for either non-thermal bremsstrahlung or X-ray synchrotron emission.

ACKNOWLEDGEMENTS

JV is supported by the NASA through Chandra Postdoctoral Fellowship Award number PF0-10011 issued by the Chandra X-ray Observatory Center.

REFERENCES

- Bocchino, F., Vink, J., Favata, F., et al., 2000, A&A, 360, 671
 Borkowski, K.J., Rho J., Reynolds S.P., Dyer K. 2001, ApJ, 550, 334
 Bykov, A.M., Uvarov, Y.A., 1999, JETP, 88, 465
 Dickel, J.R., Strom, R.G., Milne, D.K. 2000, ApJ, 546, 447
 Dyer, K., et al., 2002, these proceedings
 Ghavamian, P. 1999, Ph.D. thesis, Rice University
 Ghavamian, P., Raymond, J., Smith, R.C., Hartigan, P. 2001, ApJ, 547, 995
 Green D.A. 2000, 'A Catalogue of Galactic Supernova Remnants (2000 August version)', (<http://www.mrao.cam.ac.uk/surveys/snrs/>).
 Haug, E. 1997, A&A, 326, 417
 Itoh, H. 1984, ApJ, 285,601
 Jansen, F., et al. 2001, A&A, 365, L1
 Koyama, K., Petre, R., Gotthelf, E., et al. 1995, Nat, 378, 255
 Laming, J. M., Raymond, J., McLaughlin, B., Blair, W. 1996, ApJ, 472, 267
 Laming, J. M. 2001, ApJ, 563, 828
 Mewe, R., Kaastra, J., Liedahl, D.A. 1995, Legacy 6, 16
 Mewe, R. 1999, in X-ray Spectroscopy in Astrophysics, ed. J. van Paradijs and J. Bleeker (Springer-Verlag)
 Milne, D. K., Dickel, J. R. 1975, Aust.J.Phys., 28, 209
 Porquet, D., Arnaud, M., Decourchelle, A. 2001, A&A, 373, 1110
 Strüder, L., et al. 2001, A&A, 365, L18
 Vink, J., Kaastra J., Bleeker, J. 1997, A&A, 328, 628